

Effect of stress-induced phase transformation on nanomechanical properties of sputtered amorphous carbon films

W. Lu and K. Komvopoulos

Department of Mechanical Engineering
University of California
Berkeley, California 94720

Abstract

The nanomechanical properties of radio-frequency sputtered ultrathin carbon films measured by surface force microscopy were correlated to the carbon bonding structures analyzed by x-ray photoelectron and Auger electron spectroscopy. The films consisted of amorphous carbon (a-C) comprising both trigonal (sp^2) and tetrahedral (sp^3) carbon hybridizations. The sp^3 carbon content in the a-C materials of films with nanohardness of 19-40 GPa was found to be in the range 22-28%. From the variations of the binding energy of core level Ar 2p electrons and the sp^3 carbon content with the film Ar content, a stress-induced phase transformation from sp^2 to sp^3 carbon was determined at a compressive residual stress of about 14 GPa. Film hardening occurs due to material densification, which is controlled by the intensity of energetic Ar^+ bombardment and the flux ratio of incoming C atoms and Ar^+ ions during film growth. The results of this study elucidate the underlying hardening mechanism in ultrathin sputter-deposited carbon films.

Introduction It is well established that the mechanical properties of carbon films (e.g., hardness) depend strongly on the film microstructure (e.g., atomic bonding, such as ratio of tetrahedral to trigonal carbon bonding, referred to as sp^3/sp^2) that is affected by the deposition conditions. Raman spectroscopy has been used to estimate the sp^2 and sp^3 carbon contents in sputtered amorphous carbon (a-C) films,¹ and to evaluate the residual stress in cathodic arc a-C films.² X-ray photoelectron spectroscopy (XPS) has also been used to study the composition and microstructure of thin a-C films synthesized by different methods. Photoelectrons from core levels can yield information about the composition of the surface layer, chemical and mechanical environment of atoms in the near-surface region³⁻⁵ (such as residual stress due to energetic ion bombardment during film growth), and atomic bonding of carbon materials.^{6,7} Diaz et al.⁷ estimated the sp^2 and sp^3 carbon fractions in a-C films deposited on silicon substrates by pulsed laser evaporation of graphite targets by deconvoluting the core level C 1s XPS spectra. For film hardness of 40 and 22 GPa, the corresponding sp^3 carbon content was about 28.6 and 20%. Lascovich et al.^{8,9} evaluated the sp^2/sp^3 ratio of pure and hydrogenated a-C films fabricated by dual ion beam sputtering by measuring the binding energy shift of the C 1s XPS transition. A 25% sp^3 carbon content was determined for pure a-C films. The objective of this study was to examine the nanohardness dependence of ultrathin carbon films on carbon bonding structures and to analyze the effects of residual compressive stress and material densification due to Ar⁺ bombardment on film hardening.

Experimental Procedures. Thin a-C films 10-70 nm in nominal thickness were deposited on clean and smooth Si(100) substrates by non-magnetron radio frequency (rf) sputtering. High-purity graphite target and pure Ar gas were used for film deposition. The rf power P , substrate bias voltage V_s , and deposition time t were varied in order to obtain films possessing different compositions, thickness,

residual stress, and nanomechanical properties (Table I). The sputtering system and deposition procedures have been described elsewhere.¹⁰ The film nanohardness and elastic modulus were measured with a surface force microscope using a ~20-nm-radius diamond tip and maximum contact loads of 20 μN .^{6,10} Due to the small indentation depth-to-film thickness ratio h_c/d , most of the measured nanomechanical properties (especially nanohardness) are fairly close to the true film properties.¹¹ Thus, the measured nanohardness can be associated with the film microstructure.

The films were characterized by x-ray photoelectron spectroscopy (XPS) and x-ray Auger electron spectroscopy (XAES) using a Kratos Analytical XPS spectrometer with an AlK α monochromatic x-ray source ($h\nu = 1486.6 \text{ eV}$).^{3,6,10} To avoid possible surface and microstructure changes, the samples were not subjected to Ar⁺ bombardment or heating prior to the XPS. To prevent charging, all the samples were mounted on a Cu holder using Ag colloid conductive glue and the irradiated surface areas were neutralized with sufficient electrons. The constituents of carbon film materials (i.e., sp^2 and sp^3 carbon) were determined by deconvoluting the C 1s XPS spectra (Fig. 1), after applying Shirley subtraction¹² for inelastic scattering background and fitting Gaussian distributions at characteristic binding energies using the method of Sherwood.¹³ For the integral XAES spectra of C KLL, Gaussian distributions corresponding to characteristic Auger electrons were used to fit the spectra after a 25-point Savinsky-Golay quadratic smoothing and a Shirley background subtraction, while the first-order derivative of the smoothed integral C KLL XAES spectra (Fig. 2) was obtained after a 25-point Savinsky-Golay quadratic smoothing.

Results and Discussion. Substrate biasing promoted Ar⁺ acceleration through the plasma sheath and bombardment of the film surface, thereby resulting in Ar⁺ implantation into the films. The amount of implanted Ar increased with ion current density and kinetic energy of Ar⁺ bombarding the film surface.

Thus, the Ar content depended on the intensity of Ar⁺ bombardment during film growth and the flux ratio of incoming C atoms and energetic Ar⁺ ions, which affects the film density and nanomechanical properties.^{10,14} Figure 3 shows that the film nanohardness changes with increasing Ar content. These very small amounts of Ar cannot yield such a pronounced hardening effect. Energetic Ar⁺ bombardment during film deposition is believed to be the prime cause of film hardening. Hence, if there is a dispersion hardening effect of the embedded Ar atoms, its effectiveness depends primarily on the microstructure of the host a-C materials, which is controlled by energetic Ar⁺ bombardment during film deposition.

While the Ar content hardly affects the nanomechanical properties of the films,¹⁴ small amounts of Ar provide not only information about the plasma environment that the films were synthesized⁶ but also the residual stress in the films,^{3,4} which is related to the binding energy shift of the Ar 2p_{3/2} XPS transition. For the a-C films of this study, the binding energy of Ar 2p_{3/2} XPS transitions is between 241.3 and 242.1 eV and the full width at half magnitude (FWHM) is in the range 1.01-1.06 eV, while the binding energy of core level XPS C 1s transitions is in the narrow range 284.3-284.5 eV (Table I). These data show that energetic ion bombardment during film deposition causes the binding energy of Ar 2p_{3/2} to shift to lower values. This shift is attributed to a compressive residual stress produced in the films due to Ar⁺ bombardment.^{3,4}

The XPS C 1s spectra exhibited a long tail in the high-energy end of the spectrum and FWHM between 1.46 and 1.68 eV (Table I). These characteristics indicate that the films possess different microstructures of a-C materials. The broadening of the XPS C 1s peak is attributed to film amorphization. The binding energies of the Gaussian fits in the representative XPS spectrum shown in Fig. 1 [denoted by 1-6 and C 1s(1)-C 1s(6) in Table II] are approximately equal to 284.4, 285.4, 286.7, 288.2, 289.9, and 291.7 eV. These binding energies are correlated to different carbon bonding states,^{6,15,16} i.e., C 1s(1): sp² carbon, C 1s(2): sp³ carbon, C 1s(3): sp² carbon with neighboring N

atoms, C 1s(4): sp^3 carbon with neighboring N atoms, C 1s(5): sp^2 carbon with neighboring O and N atoms, and C 1s(6): sp^3 carbon with neighboring O and N atoms. Characteristic binding energies and corresponding percentages are given in Table II. The sp^3 carbon content is 22-28% of the total carbon material, which is in good agreement with the findings of earlier studies on similar sputtered a-C films.⁶⁻⁹

Figure 4 shows the binding energy of Ar $2p_{3/2}$ and sp^3 content in the a-C films versus Ar concentration. The sp^3 fraction increases proportionally with the Ar content, which is affected by the energetic ion bombardment intensity during deposition and the C atom-to- Ar^+ ion flux ratio. This relation between the sp^3 and Ar contents implies that energetic ion bombardment during deposition promotes sp^3 carbon formation. As shown in Fig. 4, the binding energy of Ar $2p_{3/2}$ decreases with increasing Ar content in the range 0-1.5 at%. However, at higher Ar contents, the binding energy increases, suggesting the occurrence of stress relaxation despite the increase of the ion bombardment intensity. For ~1.5 at% Ar, the biaxial compressive residual stress is in the range 12-14 GPa,⁴ which is close to the maximum compressive residual stress of 16 GPa reported previously.¹⁴ The stress relaxation for Ar content greater than ~1.5 at% and the continuous increase of the sp^3 percentage reveal a stress-induced phase transformation from sp^2 to sp^3 carbon hybridizations in the highly stressed a-C materials commencing at a critical compressive stress of about 14 GPa. This kind of stress-induced phase transformation, where a very high compressive stress causes pairs of sp^2 carbon sites to bond together to form sp^3 carbon configurations, was inferred by Schwan et al.¹⁴ to explain material densification by energetic Ar^+ bombardment during deposition and has been observed in an annealing experiment of highly stressed sputtered a-C films.³ Therefore, the increase of the sp^3 content and the development of a maximum compressive residual stress with increasing ion bombardment intensity can be attributed to a stress-induced phase transformation from sp^2 to sp^3 carbon that enhanced material densification.

The $dN(E)/dE$ XAES spectra of the a-C films (e.g., samples 4 and 5, Fig. 2) contained three characteristic peaks. The kinetic energy KE and FWHM of the three features in the Auger spectra are listed in Table III. The main peak is identified as the C KLL Auger peak with kinetic energy between 263.93 and 264.74 eV and FWHM values in the range 19.23-19.83 eV. The third peak can be clearly identified as the Ar LMM Auger peak, while the second peak is believed to be due to surface plasmon energy loss of C KLL Auger electrons leaving the surface at a kinetic energy of ~ 264.5 eV. The kinetic energy difference ΔE between the first two transitions (attributed to surface plasmon energy loss) is in the range 20.9-21.3 eV (Table III). The predicted volume and surface plasmon energies of an a-C film with 2.6 g/cm^3 density are 26.83 and 18.97 eV, respectively.¹⁷ Since the escape length of C KLL Auger electrons with kinetic energy ~ 264.5 eV is $\sim 2 \text{ nm}$,¹⁸ the energy loss due to excitation of the plasma oscillation should be between 18.97 and 26.83 eV, which is in fair agreement with the kinetic energy loss values given in Table III. Since the plasmon energy is proportional to the square root of the electron concentration (i.e., film density), the plasmon energy increases with film density. Figure 5 shows the film nanohardness and binding energy of Ar $2p_{3/2}$ electron versus surface plasma energy loss. The second-order polynomial function fit (correlation coefficient = 0.985) to the surface plasmon energy loss and film hardness data suggests that the material density controls the film nanohardness. Therefore, to increase the film hardness, the deposition conditions must be optimized to maximize the carbon film density. The variation of the Ar $2p_{3/2}$ binding energy with energy loss (Fig. 5) indicates that energetic Ar^+ bombardment during film deposition not only promotes film densification but also introduces a compressive residual stress in the films. However, a maximum compressive residual stress exists, which is associated with a stress relaxation mechanism involving a stress-induced phase transformation from sp^2 to sp^3 carbon hybridization, in accord with the previous discussion.

Conclusions. In summary, the film Ar content, which depends on the intensity of Ar⁺ bombardment during deposition, yields important insight into the mechanical environment of the a-C films (e.g., residual stress). Energetic ion bombardment promotes sp^3 carbon formation, as shown by the increase of the sp^3 carbon fraction with increasing Ar content. The interdependence of the sp^3 carbon fraction, Ar content, and binding energy of Ar 2p reveals a stress-induced phase transformation from sp^2 to sp^3 carbon hybridization at a critical high compressive residual stress (~14 GPa), resulting in the formation of a denser carbon material. Hence, ion bombardment during film deposition promotes sp^3 carbon formation and film densification. This study also indicates that film hardening is due to material densification induced by energetic ion bombardment rather than the occurrence of a high compressive residual stress, suggested in several previous studies as the primary reason for the hardening of thin carbon films.

Acknowledgments. This research was supported by the Surface Engineering and Tribology Program of the National Science Foundation under Grant No. CMS-9734907, and the Computer Mechanics Laboratory at the University of California at Berkeley.

References

¹J. Schwan, S. Ulrich, V. Batori, H. Ehrhardt, and S. R. P. Silva, J. Appl. Phys. **80**, 440 (1996).

²J. W. Ager III and M. D. Drory, Phys. Rev. B **48**, 2601 (1993).

³W. Lu, K. Komvopoulos, and S. W. Yeh, J. Appl. Phys. **89**, 2422 (2001).

⁴W. Lu and K. Komvopoulos, Appl. Phys. Lett. **76**, 3206 (2000).

⁵K. S. Kim and N. Winograd, Chem. Phys. Lett. **30**, 91 (1975).

⁶W. Lu and K. Komvopoulos, J. Appl. Phys. **85**, 2642 (1999).

- ⁷J. Diaz, G. Paolicelli, S. Ferrer, and F. Comin, *Phys. Rev. B* **54**, 8064 (1996).
- ⁸J. C. Lascovich, R. Giorgi, and S. Scaglione, *Appl. Surf. Sci.* **47**, 17 (1991).
- ⁹J. C. Lascovich, and S. Scaglione, *Appl. Surf. Sci.* **78**, 17 (1994).
- ¹⁰W. Lu and K. Komvopoulos, *J. Appl. Phys.* **86**, 2268 (1999).
- ¹¹W. Lu and K. Komvopoulos, *J. Tribol.* **123**, 641 (2001).
- ¹²D. A. Shirley, *Phys. Rev. B* **5**, 4709 (1972).
- ¹³P. Sherwood, in *Practical Surface Analysis by Auger and X-ray Photoelectron Spectroscopy*, edited by D. Briggs and P. Seah (Wiley, New York, NY, 1983), p. 445.
- ¹⁴J. Schwan, S. Ulrich, H. Roth, H. Ehrhardt, S. R. P. Silva, J. Robertson, R. Samlenski, and R. Brenn, *J. Appl. Phys.* **79**, 1416 (1996).
- ¹⁵F. R. McFeely, S. P. Kowalczyk, L. Ley, R. G. Cavell, R. A. Pollak, and D. A. Shirley, *Phys. Rev. B* **9**, 5268 (1974).
- ¹⁶J. C. Lascovich and A. Santoni, *Appl. Surf. Sci.* **103**, 245 (1996).
- ¹⁷C. Kittel, *Introduction to Solid State Physics*, 4th ed. (Wiley, New York, NY, 1971).
- ¹⁸J. F. Watts, *Introduction to Surface Analysis by Electron Spectroscopy* (Oxford University Press, New York, NY, 1990).

Table I. Deposition conditions, film properties, Argon content, and binding energy (BE) of core level XPS transitions C 1s and Ar 2p_{3/2} with FWHM values of a-C films.

Sample	Deposition Conditions ^a			Film Properties				XPS Results				
	P	V_s	t	d	H	$[E/(1-n^2)]$	h_c/d	Ar (at%)	C 1s (eV)		Ar 2p _{3/2} (eV)	
	(W)	(V)	(min)	(nm)	(GPa)	(GPa)			BE	FWHM	BE	FWHM
1	500	0	5	22	20.4	142.8	0.23	1.30	284.5	1.46	241.9	1.04
2	500	-200	5	11	29.1	184.6	0.31	1.63	284.3	1.56	241.4	1.06
3	500	-200	10	39	34.3	219.1	0.07	2.03	284.4	1.68	241.5	1.01
4	750	0	5	27	19.7	132.6	0.19	0.51	284.5	1.49	242.1	1.03
5	750	-200	5	10	39.2	185.1	0.23	1.93	284.4	1.68	241.5	1.03
6	750	-200	10	69	31.8	207.5	0.04	1.54	284.3	1.59	241.3	1.06

^aAr gas flow rate = 20 sccm; working pressure = 3 mTorr.

Table II. Binding energy (BE) and fractions of characteristic peaks of core level C 1s XPS spectra and sp^3 carbon content of a-C films.

Feature	Sample											
	1		2		3		4		5		6	
	BE (eV)	%										
C 1s (1)	284.4	63.5	284.3	63.7	284.4	63.0	284.5	66.3	284.4	63.6	284.2	63.3
C 1s (2)	285.4	19.6	285.4	19.9	285.4	22.2	285.5	17.2	285.4	21.1	285.3	20.0
C 1s (3)	286.7	9.1	286.7	7.7	286.7	8.2	286.7	7.7	286.7	7.1	286.7	8.4
C 1s (4)	288.4	5.0	288.3	5.0	288.4	4.1	288.1	5.3	288.1	4.8	288.4	4.8
C 1s (5)	290.1	1.9	289.9	2.6	290.1	1.7	289.6	2.2	289.6	2.3	290.1	2.4
C 1s (6)	291.8	0.8	291.7	1.2	291.7	0.8	291.2	1.2	291.4	1.2	291.9	1.1
sp^3 (%)	25.5 ± 0.1		26.1 ± 0.7		27.1 ± 0.6		23.6 ± 1.1		27.0 ± 0.3		25.9 ± 0.3	

Table III. Kinetic energy (KE) and FWHM of decomposed main Auger transitions in the C KLL Auger spectra and kinetic energy difference (ΔE) between C KLL and A2 Auger transitions due to surface plasmon energy loss of a-C films.

Sample	C KLL		A2		Ar LMM		ΔE (eV)
	KE (eV)	FWHM (eV)	KE (eV)	FWHM (eV)	KE (eV)	FWHM (eV)	
1	264.24	19.23	243.32	21.59	221.79	19.94	20.92
2	264.45	19.81	243.33	21.62	221.73	19.96	21.12
3	264.63	19.81	243.37	21.48	222.05	19.83	21.26
4	263.93	19.51	243.03	21.66	222.33	19.76	20.90
5	264.74	19.83	243.45	21.57	222.05	19.87	21.30
6	264.55	19.74	243.34	21.50	222.30	19.91	21.21

List of Figures

- FIG. 1. Representative core level C 1s XPS spectrum of a-C films (sample 5).
- FIG. 2. First-order derivative XAES spectra (plotted in binding energy scale) of a-C films deposited under zero (sample 4) and -200 V (sample 5) substrate bias voltage.
- FIG. 3. Film nanohardness versus Ar content.
- FIG. 4. Binding energy of Ar $2p_{3/2}$ and sp^3 carbon content in a-C materials versus Ar content.
- FIG. 5. Film nanohardness and binding energy of Ar $2p_{3/2}$ versus surface plasmon energy loss.

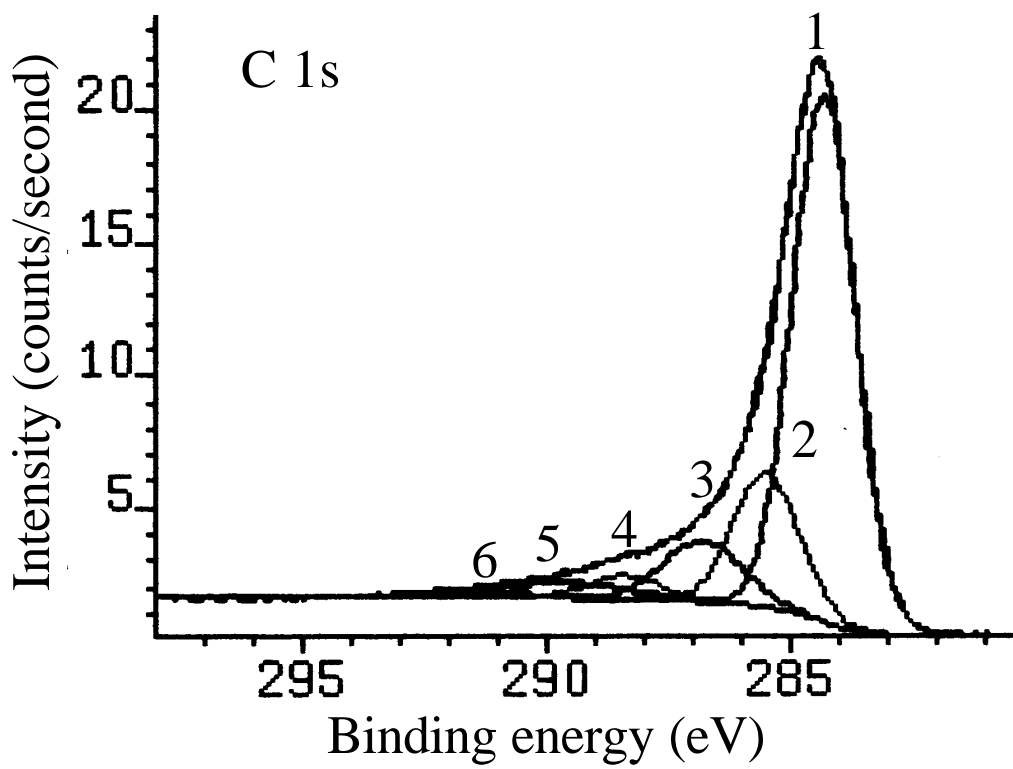


Figure 1

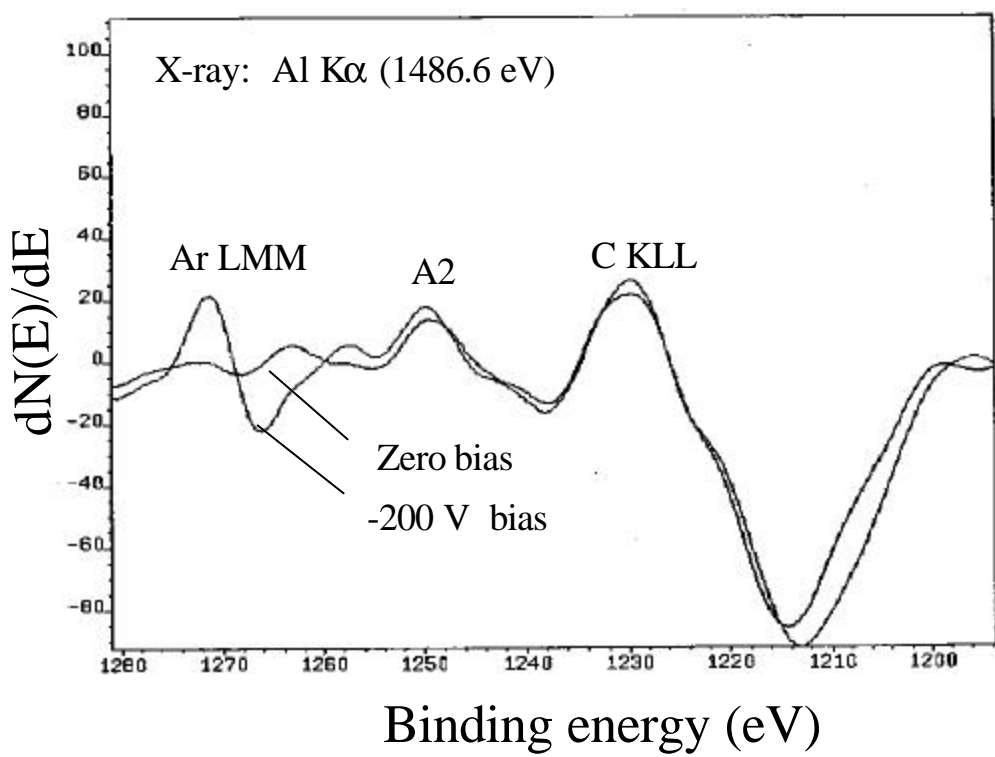


Figure 2

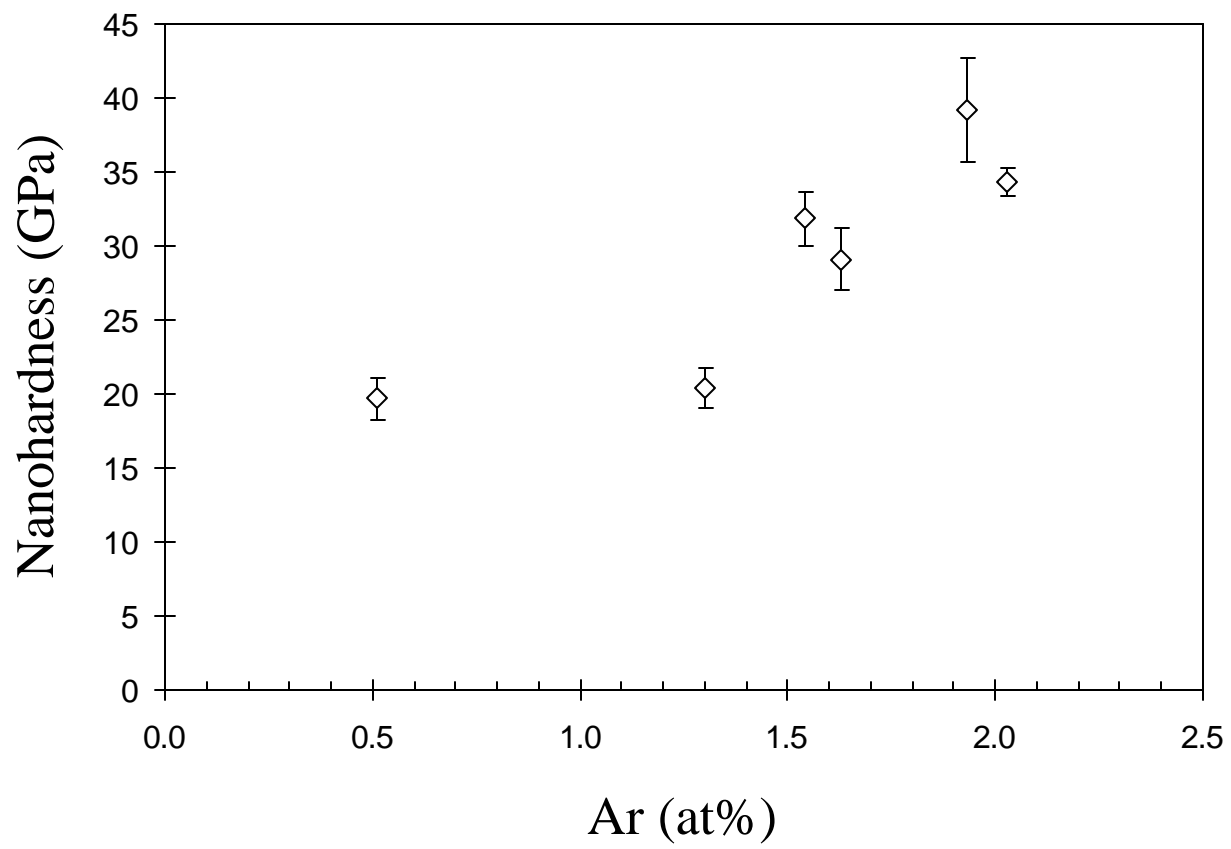


Figure 3

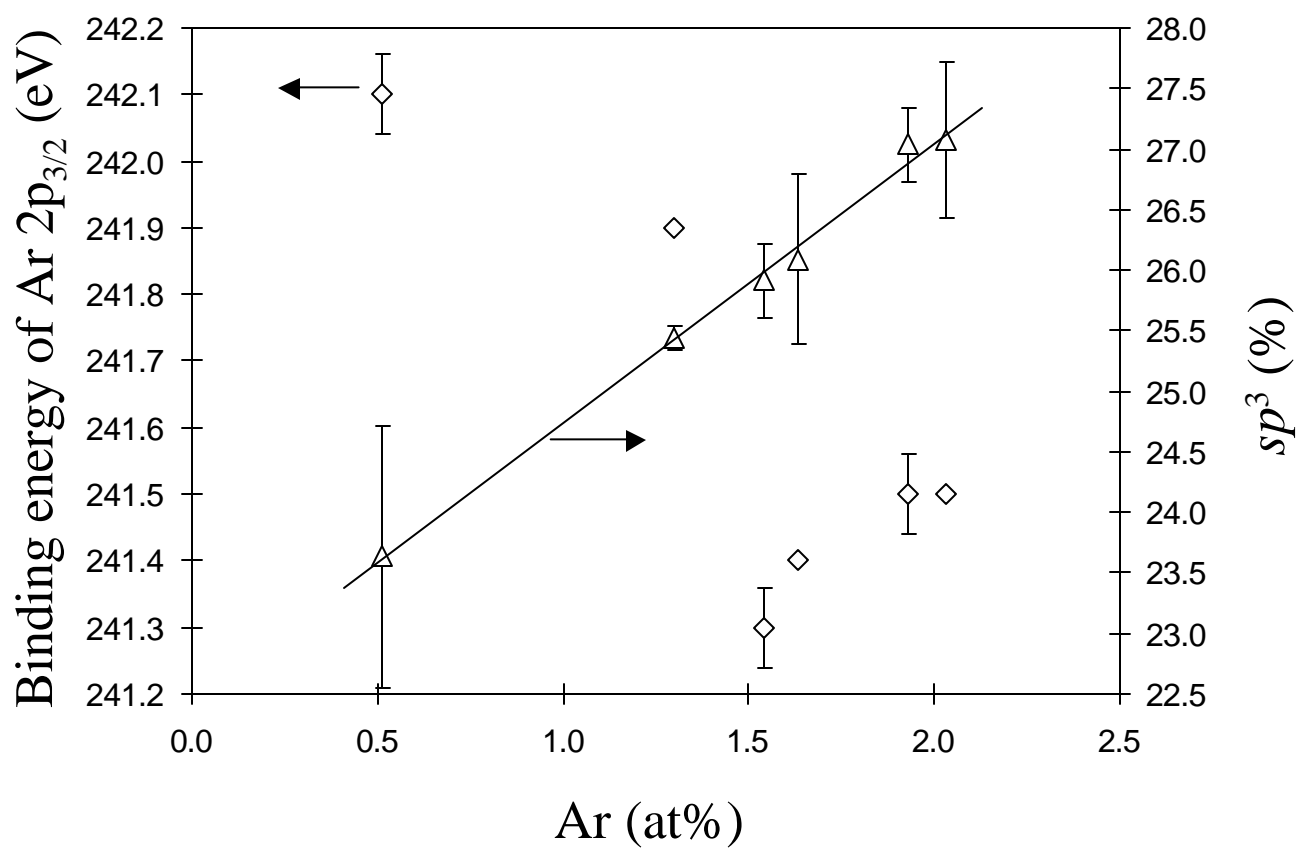


Figure 4

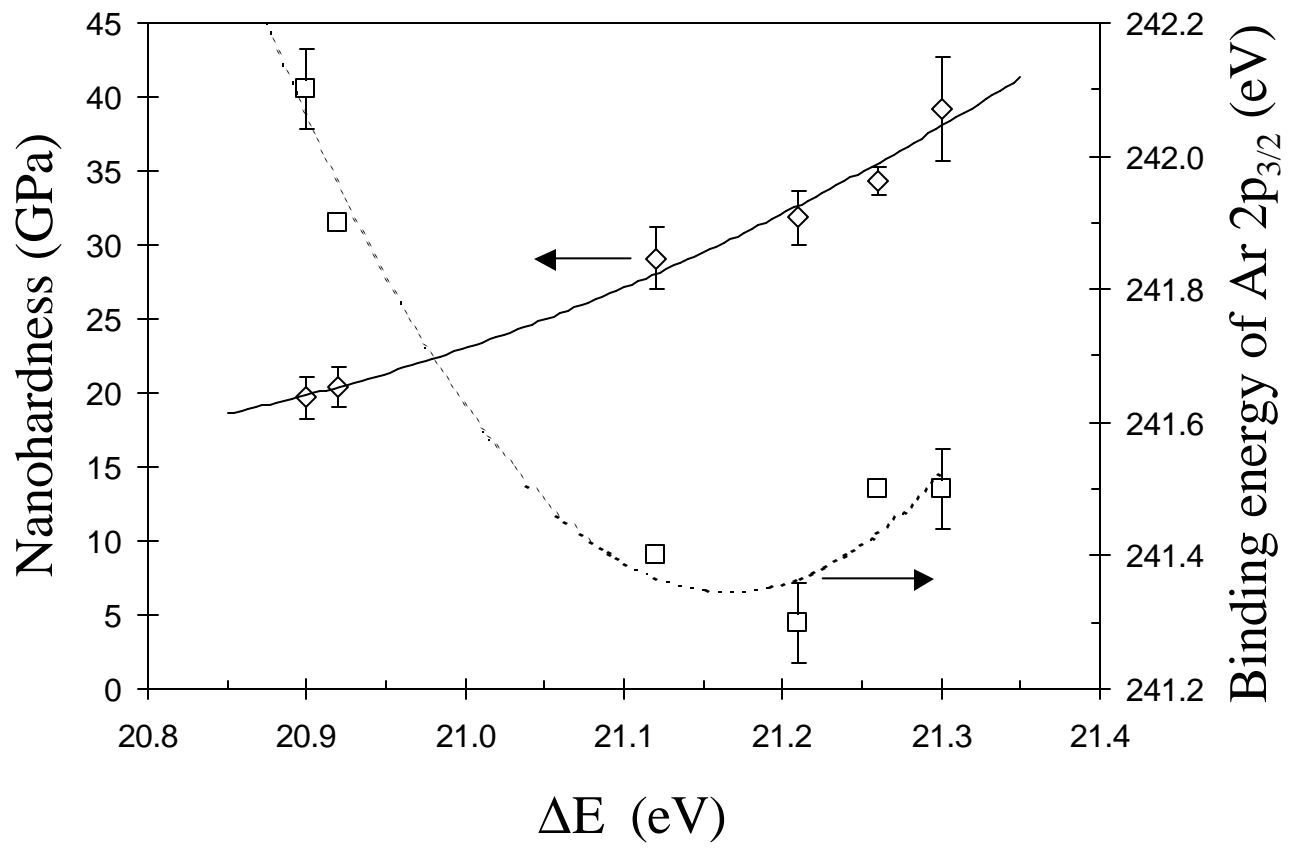


Figure 5